

Modelling size dependent bending behavior of cracked magneto electro piezoelectric nanobeam under Hygro-Thermal loads

Selvapandi Muthulakshmi[†], Rajendran Selvamani^{‡*}, Farzad Ebrahimi[§]

^{†,‡}Department of Mathematics, Karunya Institute of Technology and Sciences, Coimbatore 641114, Tamil Nadu, India

[§]Mechanical Engineering department, faculty of engineering, Imam Khomeini International University, Qazvin, Iran P.O.B. 16818-34149

Email(s): smuthulakshmi0198@gmail.com, selvam1729@gmail.com, febrahimi@eng.ikiu.ac.ir

Abstract. This study is focused on the bending response of electro-magneto-elastic nanobeams exposed to hygro-thermal environments while resting on a Winkler–Pasternak elastic foundation, utilizing non-local elasticity theory. The governing equations are formulated within the framework of parabolic third-order shear deformation beam theory and derived using Hamilton’s principle. An open crack is modeled as a rotational spring to represent its local flexibility, and its influence is integrated into the analytical solution. A comprehensive parametric study examines how the nonlocal parameter, crack severity and position, aspect ratio, hygro-thermal and magneto-electro-mechanical loadings, influence the deflection characteristics of nanobeams. The findings reveal that cracks, boundary conditions, nonlocal effects, and beam geometry significantly influence the dimensionless deflection behavior of nanoscale structures.

Keywords: Bending, nonlocal elasticity theory, hygro-thermal loading, magneto-electro piezoelectric nanobeam, crack.

AMS Subject Classification 2010: 74A25, 74F15, 74J30.

1 Introduction

The first electro–magneto–elastic hybrid material, combining electromechanical and magnetomechanical segments, was developed in the 1970s by Van den Boomgard et al. [36]. Since then, electro–magneto–elastic nanomaterials such as $BiFeO_3$, $BiTiO_3-CoFe_2O_4$, and $NiFe_2O_4-PZT$ have garnered significant attention in nanoscale research, as reported by Zhao et al. [39], Ramirez et al. [31], Wang et al. [37],

*Corresponding author

Received: 13 August 2025/ Revised: 05 November 2025/ Accepted: 08 January 2026

DOI: [10.22124/jmm.2026.31394.2819](https://doi.org/10.22124/jmm.2026.31394.2819)

Prashanthi et al. [28], and Ke et al. [19]. Owing to the remarkable mechanical strength and multi-functional capabilities of these nanostructures, it is essential to thoroughly analyze and understand their mechanical behavior before developing advanced design applications. However, classical continuum theories remain valid only down to a certain size scale, beyond which they fail to accurately predict nanoscale responses.

Mindlin [23] introduced the concept of microstructure in linear elasticity, forming the foundation for generalized continuum theories such as couple stress and micropolar elasticity. Incorporating rotational degrees of freedom and internal length scales enabled the prediction of size-dependent behavior beyond classical elasticity, which is essential for analyzing micro- and nanoscale structures. Building on Mindlin's ideas, Eringen developed generalized continuum and nonlocal elasticity theories [11–15] that incorporate microstructural and long-range interaction effects. In his micromorphic and nonlocal polar formulations, the stress at a point depends on the strain field within a finite region, effectively capturing size-dependent behavior. His mathematically rigorous models established the theoretical basis for modern nonlocal and size-dependent analyses. Later, Challamel and Wang [6, 21] resolved the paradox in nonlocal elasticity by proving that the apparent softening of cantilever beams resulted from improper boundary conditions; with the correct integral form, nonlocal effects actually increase stiffness, aligning with physical expectations.

Peddie et al. [29] developed the Euler–Bernoulli and Timoshenko nonlocal beam theories to model nanostructures, effectively capturing size-dependent behavior through a small length-scale parameter. These models accurately predict bending and buckling responses at the nanoscale. Simsek et al. [34] extended this framework by formulating a three-unknown nonlocal beam theory that accounts for shear and longitudinal strains. Fernández-Sáez [16] further refined nonlocal analysis using Eringen's integral formulation, resolving the nonlocal paradox and providing a consistent approach for modeling nanoscale beam deflections and stresses.

Sobhy [35] analyzed the buckling and vibration of functionally graded sandwich plates on elastic foundations using an exponential gradation model. Civalek et al. [5] examined microtubule bending via nonlocal Euler–Bernoulli theory, showing improved nanoscale stiffness and deflection predictions. She et al. [33] investigated wave propagation in functionally graded porous nanobeams, revealing the effects of scale, gradation, and porosity on wave behavior. Zhang et al. [38] studied the free vibration of porous FG magneto-electro-elastic microbeams under hygrothermal conditions, highlighting environmental influences on natural frequencies.

Ebrahimi and collaborators [7, 8] developed comprehensive size-dependent models for multifunctional nanoscale structures incorporating nonlocal elasticity along with thermal, piezoelectric, and magnetic effects. Their analyses of thermo–piezo-electrically actuated nanobeams under magnetic and thermal fields revealed strong coupling between electromechanical and thermal responses. Ebrahimi and Habibi [9, 10] further examined the dynamic behavior of FG-CNT reinforced plates in thermal environments, emphasizing the roles of temperature, CNT reinforcement, and field coupling on vibration characteristics. Arefi et al. [3] investigated thermo–magneto–electro–elastic graded nanobeams with piezo–magnetic layers, showing how coupled fields influence bending and buckling responses. Zheng et al. [40] analyzed nonlinear deformation in magneto-electro-elastic nanobeams resting on elastic foundations using nonlocal modified couple stress theory, demonstrating the influence of magneto-electro-mechanical coupling and foundation stiffness on deflection and stability. Khodabakhshi et al. [20] introduced a unified integro-differential nonlocal model combining integral and differential formulations for more accurate representation of size-dependent effects in nanoscale structures.

Ghorbanpour et al. [17] analyzed electro–mechanical sandwich nanoplates supported by a silica aerogel foundation, reporting that parameters such as voltage, porosity, and foundation stiffness strongly affect bending behavior. Selvamani et al. [32] examined a modified nonlocal couple stress model for magneto-thermoelastic multilayered cylinders, incorporating Hall currents and two-phase lag heat conduction to explore coupled field effects. Pehlivan et al [30] studied smart magneto–electro–elastic FGM nanosensor beams, showing that porosity and material gradation significantly influence stress, deformation, and sensing performance. Alghanmi [2] analyzed functionally graded nanobeams integrated with piezoelectric composite actuators, highlighting the combined effects of nonlocality, material gradation, and actuator coupling on deformation and stress fields.

Adams et al. [1] introduced a vibration-based non-destructive technique for assessing structural integrity by detecting changes in natural frequencies and mode shapes, establishing the foundation for vibration-based damage identification. Loya et al. [22] investigated the transverse vibration of cracked nanobeams using nonlocal elasticity, modeling cracks as rotational and shear springs to incorporate flexibility effects without physically segmenting the beam an efficient approach for nanoscale vibration analysis. Hussein et al. [18] extended this framework to multiple cracked nanobeams, showing that crack number and location significantly affect natural frequencies and dynamic behavior under various boundary conditions. Bastanfar et al. [4] analyzed cracked piezoelectric nanobeams by incorporating flexoelectric and surface energy effects within modified couple stress theory, demonstrating that these nanoscale phenomena strongly influence resonant responses. Norouzzadeh and co authors [24–27] developed comprehensive nonlocal and strain gradient models for nanoscale Timoshenko beams using finite element and isogeometric formulations. Their studies revealed that small-scale effects, shear deformation, rotary inertia, and strain gradients play crucial roles in the bending, vibration, buckling, and wave propagation of nanobeams, providing reliable tools for analyzing deflection, stress distribution, and stability under both linear and nonlinear loading conditions.

Building upon previous studies, the present work investigates the bending behavior of cracked nano beams subjected to hygro–thermal loading using a refined shear deformation theory. The governing equations are formulated analytically through Hamilton’s principle in conjunction with Eringen’s nonlocal elasticity theory. The analysis explores the influences of hygro–thermal effects, magneto–electro–mechanical coupling, crack presence, various boundary conditions, and Winkler–Pasternak foundation parameters on the beam’s bending response. The crack is represented by a rotational spring, enabling accurate incorporation of its flexibility into the analytical model.

2 Mathematical formulation

According to the refined third-order beam theory with parabolic shear deformation, at any position along the beam, the displacement field is considered to be of the form

$$\begin{aligned} u_x(x, z) &= u(x) + \varphi(x)z - \left(\frac{\partial w}{\partial x} + \varphi(x) \right) \alpha z^3, \\ u_z(x, z) &= w(x). \end{aligned} \quad (1)$$

The displacement components w and u are defined in the mid-surface along the x and z directions, respectively, while φ is interpreted as the overall rotational deformation of the cross section, α is the constant co-efficient.

Based on the parabolic beam formulation, the nonzero strain terms are derived through the strain displacement relationship as follows:

$$\varepsilon_{xx} = \varepsilon_{xx}^{(0)} + z\varepsilon_{xx}^{(1)} + z^3\varepsilon_{xx}^{(3)}, \quad \gamma_{xz} = \gamma_{xz}^{(0)} + z^2\gamma_{xz}^{(2)}, \quad (2)$$

where

$$\begin{aligned} \varepsilon_{xx}^{(0)} &= \frac{\partial u}{\partial x}, \quad \varepsilon_{xx}^{(1)} = \frac{\partial \psi}{\partial x}, \quad \varepsilon_{xx}^{(3)} = -\alpha \left(\frac{\partial \phi}{\partial x} + \frac{\partial^2 w}{\partial x^2} \right), \\ \gamma_{xz}^{(0)} &= \varphi + \frac{\partial w}{\partial x}, \quad \gamma_{xz}^{(2)} = -\beta \left(\varphi + \frac{\partial w}{\partial x} \right), \text{ and } \beta = \frac{4}{h^2}. \end{aligned} \quad (3)$$

Based on Maxwell's equations, the interrelation among the electric field components (E_x, E_z), the electric potential ϕ , the magnetic field components (Q_x, Q_z), and the magnetic potential ψ were derived, as outlined by Ke et al. [19]:

$$E_x = -\phi_{,x} = \cos(\xi z) \frac{\partial \phi}{\partial x}, \quad Q_x = -\psi_{,x} = \cos(\xi z) \frac{\partial \psi}{\partial x}, \quad (4)$$

$$E_z = -\phi_{,z} = \sin(\xi z) \xi - \frac{2\nu}{h}, \quad Q_z = -\psi_{,z} = \sin(\xi z) \xi - \frac{2\nu}{h}. \quad (5)$$

Here, $\xi = \frac{\pi}{h}$, and the symbol ν represents the externally applied electric field on the nanobeam.

By applying the extended Hamilton's principle, the governing equations are obtained in the following form:

$$\int_0^t \delta (\Pi_S - \Pi_W) dt = 0. \quad (6)$$

In this context, Π_S is defined as the total strain energy, while Π_W refers to the externally applied forces.

The first variation of Π_S is expressed as

$$\delta \Pi_S = \int \sigma_{ij} \delta \varepsilon_{ij} dv = \int (\sigma_x \delta \varepsilon_x + \sigma_{xz} \delta \gamma_{xz}) dv. \quad (7)$$

Substituting Eqs. (1)–(2) into Eq. (6) yields

$$\begin{aligned} \Pi_S &= \int_0^a \left(N \delta \varepsilon_{xx}^{(0)} + M \delta \varepsilon_{xx}^{(1)} + P \delta \varepsilon_{xx}^{(3)} + Q \delta \gamma_{xz}^{(0)} + R \delta \gamma_{xz}^{(2)} \right) dx \\ &+ \int_0^a \int_{-h/2}^{h/2} \left[\xi \sin(\xi z) D_z \delta \phi - \cos(\xi z) D_x \frac{\partial \delta \phi}{\partial x} + \xi \sin(\xi z) B_z \delta \psi - \cos(\xi z) B_x \frac{\partial \delta \psi}{\partial x} \right] dz dx. \end{aligned} \quad (8)$$

Here, N , M and Q denote the axial force, bending moment and shear force resultants, respectively, with their corresponding stress components in defined as Eq. (9) defined as follows:

$$\begin{aligned} \{N, M, P\} &= \int_{-h/2}^{h/2} \sigma_{xx} \{1, z, z^3\} dz, \\ \{Q, R\} &= \int_{-h/2}^{h/2} \sigma_{xz} \{1, z^2\} dz. \end{aligned} \quad (9)$$

The variation in the work associated with external forces, $\delta\Pi_W$, can be written in the form

$$\delta\Pi_W = \int_0^L \left[\left(N_x^0 \frac{\partial w}{\partial x} \frac{\partial}{\partial x} + \alpha P \frac{\partial^2}{\partial x^2} - k_W w + k_P \frac{\partial^2}{\partial x^2} \right) \delta w - N \delta \varepsilon_{xx}^{(0)} - \bar{M} \frac{\partial \delta \psi}{\partial x} - \bar{Q} \delta \gamma_{xz}^{(0)} \right] dx, \quad (10)$$

where $\bar{Q} = Q - R\beta$, $\bar{M} = M - P\alpha$, and k_P, k_W are the shear and linear coefficients of the elastic medium N^B, N^E, N^T, N^H magnetic and electric, thermal and hygro-thermal loading, respectively. Accordingly, $N_x^0 = N^B + N^E - N^H - N^T$,

$$N^E = - \int_{-h/2}^{h/2} \frac{2V}{h} e_{31} dz, \quad (11)$$

$$N^B = - \int_{-h/2}^{h/2} \frac{2\Omega}{h} e_{31} dz, \quad (12)$$

$$N^T = \int_{-h/2-h_0}^{h/2-h_0} (\alpha \Delta T) dz, \quad (13)$$

$$N^H = b \int_{-h/2-h_0}^{h/2-h_0} (\beta \Delta H) dz, \quad (14)$$

and $(\alpha \Delta T)$ and $(\beta \Delta H)$ represent the thermal and moisture expansion effects, respectively. Here, α and β are the coefficients of thermal and moisture expansion, while T and H denote the temperature and moisture variations, respectively.

By inserting Eqs. (10) and (8) into Eq. (6), performing integration by parts, and grouping terms with $\delta u, \delta w, \delta \psi$, and $\delta \phi$, the governing equations are obtained as

$$\frac{\partial N_x}{\partial x} = 0, \quad (15)$$

$$\frac{\partial^2 \bar{M}}{\partial x^2} - \bar{Q} = 0, \quad (16)$$

$$\frac{\partial \bar{Q}}{\partial x} - (N^E + N^B + N^T + N^H) \frac{\partial^2 w}{\partial x^2} + \alpha \frac{\partial^2 P}{\partial x^2} - k_W w + k_P \frac{\partial^2 w}{\partial x^2} = 0, \quad (17)$$

$$\int_{-h/2}^{h/2} \left[\cos(\xi z) \frac{\partial D_x}{\partial x} + \xi \sin(\xi z) D_z + \cos(\xi z) B_x \frac{\partial \delta \psi}{\partial x} + \xi \sin(\xi z) B_z \delta \psi \right] dz = 0. \quad (18)$$

3 Nonlocal elasticity framework

The nonlocal model can be extended to magneto-electro-thermo-hydro-elastic nanobeams as follows:

$$\sigma_{ij} - (e_a)^2 \nabla^2 \sigma_{ij} = [C_{ijkl} \varepsilon_{kl} - e_{mij} E_m - q_{nij} H_n - \alpha_{ij} T - \beta_{ij} H], \quad (19)$$

$$D_{ij} - \nabla^2 D_{ij} (e_0 a)^2 = [k_{im} E_m + e_{ikl} \varepsilon_{kl} + d_{in} H_n], \quad (20)$$

$$B_i - \nabla^2 B_i (e_0 a)^2 = [d_{im} E_m + q_{ikl} \varepsilon_{kl} + \varkappa_{in} H_n], \quad (21)$$

$$p_i - \nabla^2 p_i (e_0 a)^2 = [\epsilon_0 \chi_{ij} E_j + e_{ikt} \epsilon_{kl}]. \quad (22)$$

Also, χ_{ij} is the relative dielectric susceptibility, c_{ijkl} is the elastic stiffness tensor, d_{im} and d_{in} are the magneto–electric coupling coefficients, and e_{mij} represents the piezoelectric coupling coefficients.

The nonlocal parameter $e_0 a$ is introduced to characterize the scale-dependent behavior of nanostructures. Here, ∇^2 denotes the Laplacian operator.

The stress relationship is formulated as follows:

$$(1 - \mu^2 \nabla^2) \sigma_{xx} = [C_{11} \epsilon_{xx} - e_{31} E_z - q_{31} H_z - \alpha_T \Delta T - \beta_H \Delta H], \quad (23)$$

$$\sigma_{xz} (1 - \mu \nabla^2) = [-e_{15} E_x - q_{15} H_x + C_{55} \gamma_{xz}], \quad (24)$$

$$D_x (1 - \mu \nabla^2) = [k_{11} E_x + d_{11} H_x + e_{15} \gamma_{xz}], \quad (25)$$

$$D_z (1 - \mu \nabla^2) = [k_{33} E_z + d_{33} H_z + e_{31} \epsilon_{xx}], \quad (26)$$

$$B_x (1 - \mu \nabla^2) = [d_{11} E_x + \varkappa_{11} H_x + q_{15} \gamma_{xz}], \quad (27)$$

$$B_z (1 - \mu \nabla^2) = [d_{33} E_z + \varkappa_{33} H_x + q_{31} \epsilon_{xx}]. \quad (28)$$

Integrating Eqs. (23)–(28) over the nanobeam's cross-sectional area yields the corresponding nonlocal relations for the refined beam model. Furthermore, the normal forces and bending moments induced by the electric field can be expressed as follows:

$$N - \mu \frac{\partial^2 N}{\partial x^2} = A_{xx} \frac{\partial u}{\partial x} + (B_{xx} - \alpha E_{xx}) \frac{\partial \phi}{\partial x} - \alpha E_{xx} \frac{\partial^2 w}{\partial x^2} + A_{31} \phi + G_{31} \psi - N^E - N^B + N^T + N^H, \quad (29)$$

$$M - \mu \frac{\partial^2 M}{\partial x^2} = B_{xx} \frac{\partial u}{\partial x} + (D_{xx} - \alpha F_{xx}) \frac{\partial \phi}{\partial x} - \alpha F_{xx} \frac{\partial^2 w}{\partial x^2} + B_{31} \phi + Q_{31} \psi, \quad (30)$$

$$P - \mu \frac{\partial^2 P}{\partial x^2} = E_{xx} \frac{\partial u}{\partial x} + (F_{xx} - \alpha H_{xx}) \frac{\partial \phi}{\partial x} - \alpha H_{xx} \frac{\partial^2 w}{\partial x^2} + E_{31} \phi + J_{31} \psi, \quad (31)$$

$$Q - \mu \frac{\partial^2 Q}{\partial x^2} = (A_{xz} - \beta D_{xz}) \left(\frac{\partial w}{\partial x} + \phi \right) - F_{11} \frac{\partial \phi}{\partial x}, \quad (32)$$

$$R - \mu \frac{\partial^2 R}{\partial x^2} = (D_{xz} - \beta F_{xz}) \left(\frac{\partial w}{\partial x} + \phi \right) - F_{33} \frac{\partial \phi}{\partial x}, \quad (33)$$

$$\int_{-h/2}^{h/2} \left(D_x - \mu \frac{\partial^2 D_x}{\partial x^2} \right) \cos(\xi z) dz = (F_{11} - \beta F_{33}) \left(\frac{\partial w}{\partial x} + \phi \right) + F_{11} \frac{\partial \phi}{\partial x}, \quad (34)$$

$$\int_{-h/2}^{h/2} \left(D_z - \mu \frac{\partial^2 D_z}{\partial x^2} \right) \sin(\xi z) \xi dz = A_{31} \frac{\partial u}{\partial x} + (B_{31} - \alpha E_{31}) \frac{\partial \psi}{\partial x} - \alpha E_{31} \frac{\partial^2 w}{\partial x^2} - F_{33} \phi, \quad (35)$$

$$\int_{-h/2}^{h/2} \left(B_x - \mu \frac{\partial^2 B_x}{\partial x^2} \right) \cos(\xi z) dz = (\varkappa_{11} - \beta \varkappa_{33}) \left(\frac{\partial w}{\partial x} + \phi \right) + \varkappa_{11} \frac{\partial \psi}{\partial x}, \quad (36)$$

$$\int_{-h/2}^{h/2} \left(B_z - \mu \frac{\partial^2 B_z}{\partial x^2} \right) \xi \sin(\xi z) dz = G_{31} \frac{\partial u}{\partial x} + (Q_{31} - \alpha J_{31}) \frac{\partial \psi}{\partial x} - \alpha J_{31} \frac{\partial^2 w}{\partial x^2} - \varkappa_{33} \psi. \quad (37)$$

in which

$$\{A_{11}, B_{11}, D_{11}, E_{xx}, F_{xx}, H_{xx}\} = \int_{-h/2}^{h/2} c_{11} \{z^6, z^4, z^3, z^2, z, 1\} dz, \quad (38)$$

$$\{A_{xz}, D_{xz}, F_{xz}\} = \int_{-h/2}^{h/2} c_{55} \{z^4, z^2, 1\} dz, \quad (39)$$

$$\{A_{31}, B_{31}, E_{31}\} = \int_{-h/2}^{h/2} \xi \{z^3, z, 1\} e_{31} \sin(\xi z) dz, \quad (40)$$

$$(F_{11}, F_{33}) = \int_{-h/2}^{h/2} (\cos^2(\xi z) s_{11}, \xi^2 \sin^2(\xi z) s_{33}) dz, \quad (41)$$

$$(G_{31}, Q_{31}, J_{31}) = \int_{-h/2}^{h/2} \xi \sin(\xi z) q_{31} \{z^3, z, 1\} dz, \quad (42)$$

$$(\varkappa_{11}, \varkappa_{33}) = \int_{-h/2}^{h/2} (\cos^2(\xi z) \varkappa_{11}, \xi^2 \sin^2(\xi z) \varkappa_{33}) dz. \quad (43)$$

By substituting Eqs. (38)–(43) into Eqs. (15)–(16), the displacement-based field equations for the nonlocal strain gradient nanobeam under an electric field are obtained as:

$$\frac{\partial N}{\partial x} = A_{xx} \frac{\partial u}{\partial x} + K_{xx} \frac{\partial \phi}{\partial x} - \alpha E_{xx} \frac{\partial^2 w}{\partial x^2} + A_{31} \phi + G_{31} \psi, \quad (44)$$

$$\begin{aligned} \frac{\partial^2 \bar{M}}{\partial x^2} - \bar{Q} &= (B_{xx} - \alpha E_{xx}) \frac{\partial^2 u}{\partial x^2} + (D_{xx} - \alpha F_{xx}) \frac{\partial^2 \psi}{\partial x^2} - \alpha (F_{xx} - \alpha H_{xx}) \frac{\partial^3 w}{\partial x^3} \\ &+ k_w \frac{\partial w}{\partial x} - k_P \frac{\partial^3 w}{\partial x^3} + (B_{31} - \alpha E_{31}) \frac{\partial \phi}{\partial x} + (Q_{31} - \alpha J_{31}) \frac{\partial \psi}{\partial x} \\ &- \mu \left[(-N^E - N^B + N^T + N^H) \frac{\partial^3 w}{\partial x^3} - \alpha \frac{\partial^3 P}{\partial x^3} + k_w \frac{\partial w}{\partial x} - k_P \frac{\partial^2 w}{\partial x^2} \right] \\ &- (A_{xz} - \beta D_{xz}) \left(\frac{\partial w}{\partial x} + \phi \right) - F_{11} - \beta F_{33} \frac{\partial \phi}{\partial x}, \end{aligned} \quad (45)$$

$$\begin{aligned} \frac{\partial \bar{Q}}{\partial x} &= (A_{xz} - \beta D_{xz}) \left(\frac{\partial^2 w}{\partial x^2} + \frac{\partial \phi}{\partial x} \right) - (F_{11} - \beta F_{33}) \frac{\partial^2 \phi}{\partial x^2} \\ &+ \mu \left[(N^E + N^B - N^T - N^H) \frac{\partial^3 w}{\partial x^3} - \alpha \frac{\partial^3 P}{\partial x^3} + k_w \frac{\partial w}{\partial x} - k_P \frac{\partial^3 w}{\partial x^3} \right], \end{aligned} \quad (46)$$

$$\left(\phi + \frac{\partial w}{\partial x} \right) (F_{11} - \beta F_{33}) + \frac{\partial \phi}{\partial x} F_{11} + \frac{\partial u}{\partial x} A_{31} + \frac{\partial \psi}{\partial x} (B_{31} - \alpha E_{31}) - \frac{\partial^2 w}{\partial x^2} \alpha E_{31} - \phi F_{33} = 0, \quad (47)$$

$$\left(\phi + \frac{\partial w}{\partial x} \right) (\varkappa_{11} - \beta \varkappa_{33}) + \frac{\partial \psi}{\partial x} \varkappa_{11} + \frac{\partial u}{\partial x} + G_{31} + \frac{\partial \psi}{\partial x} (Q_{31} - \alpha J_{31}) - \frac{\partial^2 w}{\partial x^2} \alpha J_{31} - \psi \varkappa_{33} = 0. \quad (48)$$

4 Solution method

The displacement components are expressed as time-harmonic function as follows:

$$u = \sum_{n=1}^{\infty} U_n \frac{\partial X_n(x)}{\partial x} e^{i\omega_n t}, \quad (49)$$

$$\varphi = \sum_{n=1}^{\infty} \varphi_n X_n(x) e^{i\omega_n t}, \quad (50)$$

$$w = \sum_{n=1}^{\infty} X_n(x) W_n e^{i\omega_n t}, \quad (51)$$

$$\psi = \sum_{n=1}^{\infty} X_n(x) \psi_n e^{i\omega_n t}, \quad (52)$$

$$\phi = \sum_{n=1}^{\infty} \phi_n X_n(x) e^{i\omega_n t}. \quad (53)$$

The coefficients u_n , φ , w , ϕ and ψ are derived as ($\alpha = \pi m/a$, $\beta = n\pi/b$):

$$[K] \begin{Bmatrix} u_n \\ \varphi \\ w \\ \psi \\ \phi \end{Bmatrix} = \begin{Bmatrix} 0 \\ Q_n \left(\frac{n^2 \pi^2}{L^2} \mu + 1 \right) \\ Q_n \left(\frac{n^2 \pi^2}{L^2} \mu + 1 \right) \\ 0 \\ 0 \end{Bmatrix}. \quad (54)$$

Here $[K]$ and $[F]$ denote the stiffness and loading matrices of the nanobeam, respectively, that

$$\begin{aligned} K_{1,1} &= \alpha_1 A_{xx}, & K_{1,2} &= \alpha_6 K_{xx}, & K_{1,3} &= \alpha_2 E_{xx}, & K_{1,4} &= \alpha_3 A_{31}, & K_{1,5} &= \alpha_3 G_{31}, \\ K_{2,1} &= (B_{xx} - \alpha E_{xx}) \alpha_6, & K_{2,2} &= (D_{xx} - \alpha F_{xx}) \alpha_6 + (A_{xx} - \beta D_{xz}) \alpha_5 - (F_{11} - \beta F_{33}) \alpha_3, \\ K_{2,3} &= \alpha_3 k_w - \alpha_2 k_p + \alpha_6 (F_{xx} - \alpha H_{xx}) + \alpha_2 \mu (-N^B - N^E - N^T - N^H) - \alpha_6 k_p + \alpha_3 k_w - \alpha_3 (A_{xx} - \beta D_{xz}), \\ K_{2,4} &= (B_{31} - \alpha E_{31}) \alpha_3, & K_{2,5} &= (Q_{31} - \alpha J_{31}) \alpha_3, \\ K_{3,2} &= (A_{xz} - \beta D_{xz}) \alpha_3, & K_{3,3} &= (A_{xz} - \beta D_{xz}) \alpha_6 + \mu [(-N^B - N^E - N^T - N^H) \alpha_2 - k_p \alpha_6] + k_w \alpha_3, \\ K_{3,4} &= (F_{11} - \beta F_{33}) \alpha_6, \\ K_{4,1} &= A_{31} \alpha_3, & K_{4,2} &= (F_{11} - \beta F_{33}) \alpha_5, & K_{4,3} &= (F_{11} - \beta F_{33}) \alpha_3 - \alpha E_{31} \alpha_6, & K_{4,4} &= F_{11} \alpha_3 - F_{33} \alpha_5, \\ K_{5,1} &= G_{31} \alpha_3, & K_{5,2} &= (\varkappa_{11} - \beta \varkappa_{33}) \alpha_5, & K_{5,3} &= (\varkappa_{11} - \beta \varkappa_{33}) \alpha_3 - \alpha J_{31} \alpha_6, & K_{5,4} &= \varkappa_{11} \alpha_3 - \varkappa_{33} \alpha_5, \\ F_{1,1} &= N \alpha_3, & F_{2,2} &= (1 - \mu \alpha_6) M - \bar{Q}, & F_{3,3} &= Q (1 - \mu \alpha_3), \end{aligned} \quad (55)$$

in which

$$\begin{aligned} \alpha_1 &= \int_0^a X'(x) X''(x) dx, & \alpha_2 &= \int_0^a X(x) X'''(x) dx, & \alpha_3 &= \int_0^a X(x) X'(x) dx, \\ \alpha_5 &= \int_0^a X(x) X'(x) dx, & \alpha_6 &= \int_0^a X(x) X''(x) dx, & \alpha_7 &= \int_0^a X(x) X'''(x) dx, \\ \alpha_{11} &= \int_0^a X'(x) X'''(x) dx. \end{aligned} \quad (56)$$

The uniformly distributed load causing bending is represented as follows:

$$q_{\text{dynamics}} = \sum_{n=1}^{\infty} \sin\left(\frac{\pi n}{L}x\right) Q_n \sin(\omega t), \quad (57)$$

$$Q_n = \frac{2}{L} \int_{x_0-c}^{x_0+c} \sin\left(\frac{\pi n}{L}x\right) q_x dx, \quad (58)$$

where Q_n are the Fourier coefficients, and $q(x) = q_0$ represents the uniform load density. Here, x_0 denotes the position of the centroid axis and t is the time variable. For a concentrated point load, the harmonic load intensity is expressed as:

$$q(x) = \sin(\omega t) \delta p(x - x_0), \quad (59)$$

$$Q_n = \frac{2p}{L} \sin\left(\frac{n\pi}{L}x_0\right), \quad (60)$$

in which δ is the Dirac delta.

Table 1: The trial functions $X_m(x)$ [35]

	Boundary conditions	The functions X_m
	At $x = 0, a$	$X_m(x)$
SS	$X_m[0] = X_m''[0] = 0$ $X_m[a] = X_m''[a] = 0$	$\sin(x\alpha)$
CC	$X_m[0] = X_m'[0] = 0$ $X_m[a] = X_m'[a] = 0$	$\sin^2(x\alpha)$

5 Crack formulation

Consider a beam with a surface crack of length a , located at a distance b from the left end. To include the crack's influence, the approach developed by several researchers [36] is expanded. In this formulation, the cracked beam is modeled as two distinct parts linked via rotational and axial elastic springs positioned at the crack site (Fig. 1). These springs are used to model the increased strain energy associated with the crack.

The strain energy U of the cracked nanobeam is given by:

$$U = \frac{1}{2} \int_0^L dx \int_A \sigma_{xx} \left(\frac{\partial u}{\partial x} - y \frac{\partial^2 v}{\partial x^2} \right) dx + \Delta \mathcal{U}_c. \quad (61)$$

With \mathcal{U}_c representing the additional strain energy due to the crack, Eq. (61) can be rewritten using the definitions from Eq. (9) in terms of the axial force N and bending moment M :

$$U = \frac{1}{2} \int_0^L \left(N \frac{\partial u}{\partial x} + M \frac{\partial^2 v}{\partial x^2} \right) dx + \Delta \mathcal{U}_c. \quad (62)$$

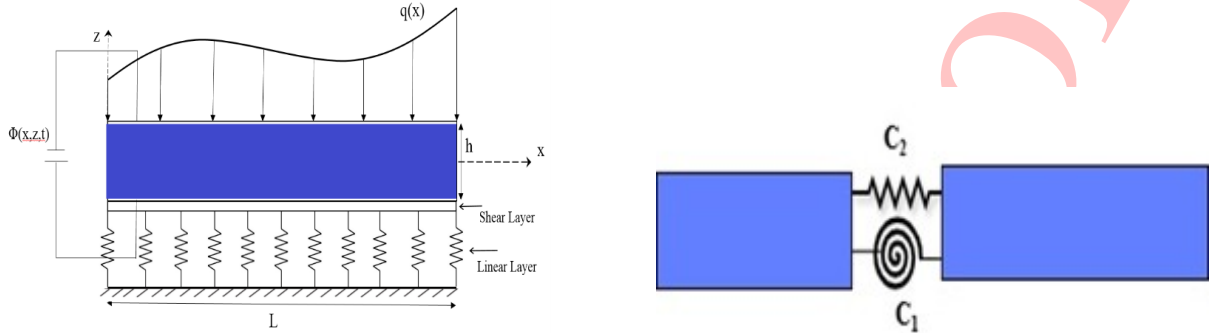


Figure 1: Geometry of representation

The additional contribution due to an edge crack is formulated based on the strain energy of an uncracked beam:

$$\Delta \mathcal{U}_c = \frac{1}{2} M(L^*, t) k_{MM} \frac{\partial^2 v}{\partial x^2} + \frac{1}{2} N(L^*, t) k_{NN} \frac{\partial u}{\partial x} + \frac{1}{2} M(L^*, t) k_{NM} \frac{\partial^2 v}{\partial x^2} + \frac{1}{2} N(L^*, t) k_{MN} \frac{\partial u}{\partial x}. \quad (63)$$

Here k_{NM} , k_{MM} , k_{MN} and k_{NN} are the flexibility constants, with k_{MN} and k_{NM} representing bending–axial coupling effects. The associated increase in strain energy is expressed as:

$$\Delta \mathcal{U}_c = \frac{1}{2} M \Delta \theta + \frac{1}{2} N \Delta u, \quad (64)$$

where $\Delta \theta$ refers to the angle of the torsional spring and Δu denotes the relative horizontal displacement at the edge crack section, Eqs. (63) and (64) are compared to derive the following relations:

$$\Delta \theta = k_{MM} \frac{\partial^2 v}{\partial x^2} + k_{MN} \frac{\partial u}{\partial x}, \quad (65)$$

$$\Delta u = k_{NN} \frac{\partial u}{\partial x} + k_{NM} \frac{\partial^2 v}{\partial x^2}. \quad (66)$$

As mentioned earlier, this study focuses on transverse free vibrations; therefore, longitudinal displacement is neglected. Furthermore, consistent with local elasticity assumptions, the crossover flexibility constants k_{MN} and k_{NM} are considered negligible, permitting the inclusion of only the bending moment related constant k_{MM} .

Thus, the slope increment at the cracked section becomes:

$$\Delta \theta = k_{MM} \frac{\partial^2 v}{\partial x^2} \Rightarrow \Delta \theta = \mathcal{K} \frac{\partial^2 v(\zeta)}{\partial x^2} \Big|_{\zeta=b}, \quad (67)$$

where $\zeta = x/L$ and $\mathcal{K} = k_{MM}/L$.

The crack-induced increment in strain energy is:

$$\Delta \mathcal{U}_c = \frac{1}{2} M \cdot \mathcal{K} \frac{\partial^2 v(\zeta)}{\partial x^2} \Big|_{\zeta=b}. \quad (68)$$

Using $M = D_{xx} \frac{\partial^2 v(\zeta)}{\partial x^2}$:

$$\Delta \mathcal{U}_c = \frac{1}{2} \mathcal{K} D_{xx} \left[\frac{\partial^2 v(\zeta)}{\partial x^2} \right]^2. \quad (69)$$

This equation models a crack by introducing a rotational spring at the crack location $\zeta = b$, where $\zeta = x/L$ is the dimensionless position along the beam. The rotational flexibility due to the crack is represented by the spring constant \mathcal{K} , and the beam's transverse displacement $v(x,t)$ is expanded in a modal form.

For modal expansion $v(x,t) = \sum_n W_n X_n(x) \phi(t)$, the crack energy term becomes:

$$\Delta \mathcal{U}_c = \frac{1}{2} \mathcal{K} D_{xx} \sum_n W_n X_n''(b)^2. \quad (70)$$

To incorporate this into the system, we compute its second variation (or equivalently, functional derivative), and this leads to the additive term in the global stiffness matrix:

$$\Delta K_{ij}^{\text{crack}} = \mathcal{K} D_{xx} X_i''(b) X_j''(b). \quad (71)$$

Thus, the total stiffness matrix is

$$[K] + [K_{\text{crack}}] \begin{Bmatrix} u_n \\ \varphi \\ w \\ \psi \\ \phi \end{Bmatrix} = \begin{Bmatrix} 0 \\ Q_n \left(\frac{1+n^2\pi^2}{2L^2} \mu \right) \\ Q_n \left(\frac{1+n^2\pi^2}{2L^2} \mu \right) \\ 0 \\ 0 \end{Bmatrix}, \quad (72)$$

where K_{crack} is the additional stiffness matrix due to the presence of a crack.

6 Numerical results and discussions

In this section, the bending response of the piezoelectric nanobeam is examined. The corresponding property of material is given in Table 2. The credibility of the current model is established through comparison of different nonlocal parameters in the absence of cracks, as shown in Table 3. A nanobeam length of $L = 10$ nm is assumed and the non-dimensional deflection is defined as:

$$W = 100 \frac{C_{11} I}{q_0 L^4}. \quad (73)$$

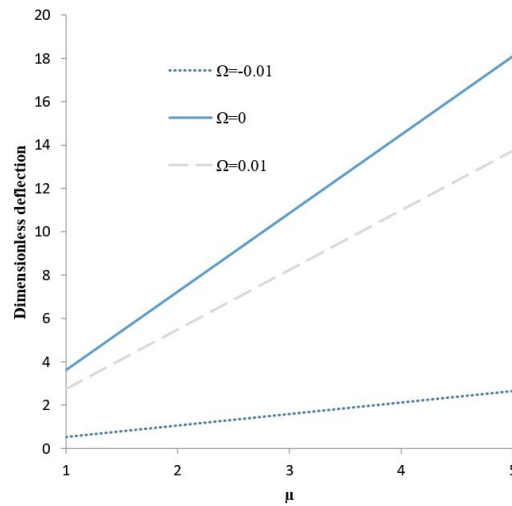
Fig. 2 illustrates how the nonlocal parameter influences the dimensionless deflection under different magnetic potentials. As the magnetic potential increases, the deflection also rises. Furthermore, as the nonlocal parameter increases, the deflection also becomes more pronounced. It is revealed that the magnetic potential significantly affects the deflection characteristics of the nanobeam.

Table 2: Material properties of BiTiO₃-CoFe₂O₄ composite materials [31]

Properties	BiTiO ₃ -CoFe ₂ O ₄
Elastic (GPa)	$c_{11} = 226, c_{12} = 125, c_{13} = 124,$ $c_{33} = 216, c_{44} = 44.2, c_{66} = 50.5$
Piezoelectric (C m ⁻²)	$e_{31} = -2.2, e_{33} = 9.3, e_{15} = 5.8$
Dielectric (10 ⁻⁹ C V ⁻¹ m ⁻¹)	$k_{11} = 5.64, k_{33} = 6.35$
Piezomagnetic (N A ⁻¹ m ⁻¹)	$q_{15} = 275, q_{31} = 290.1, q_{33} = 349.9$
Magnetolectric (10 ⁻¹² N s V ⁻¹ C ⁻¹)	$s_{11} = 5.367, s_{33} = 2737.5$
Magnetic (10 ⁻⁶ N s ² C ⁻² /2)	$\varkappa_{11} = -297, \varkappa_{33} = 83.5$
Mass density (10 ³ kg/m ³)	$\rho = 5.55, \alpha = \beta = 5 \times 10^{-6}$
Hygrothermal (/K)	$\alpha_{eff} = 1.6 \times 10^{-6}, \beta_{eff} = 26 \times 10^{-4}$

Table 3: Comparison of results for $\psi = 0.001$ and $\phi = 0.001$

L/h	μ (nm ²)	$\psi = 0.001$		L/h	μ (nm ²)	$\phi = 0.001$	
		Arefi and Zenkour [3]	Present			Arefi and Zenkour [3]	Present
10	1	3.68	3.5781	10	0	3.68	3.59892
	2	3.71	3.6482		1	1.3333	3.66921
	3	3.77	3.7302		2	1.3645	3.74018
	4	3.84	3.79011		3	1.3958	3.80234
	5	3.94	3.8952		4	1.4270	3.92011

**Figure 2:** Effect of nonlocal parameters on the dimensionless deflection under uniform loading for various magnetic potential parameters ($L/h = 10, V = 0, K_w = K_p = 20, \Delta T = 20, \Delta H = 1$)

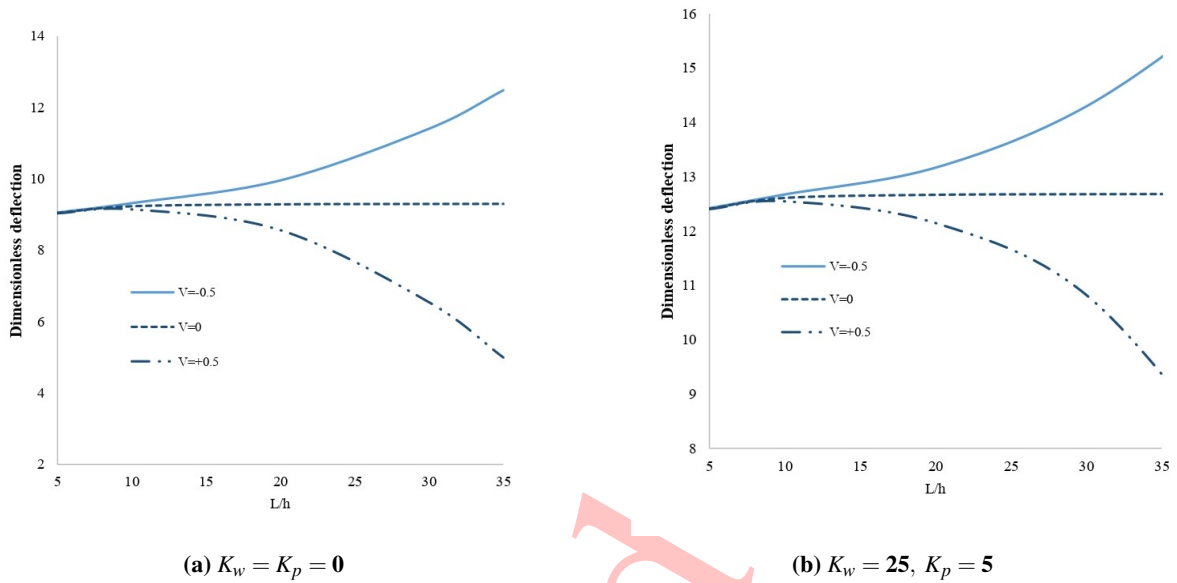


Figure 3: Effect of slenderness ratio on dimensionless deflection for uniform load for various electric voltages, without elastic foundation and with elastic foundation ($L/h = 10, \Omega = 0, \Delta T = 20, \Delta H = 1$)

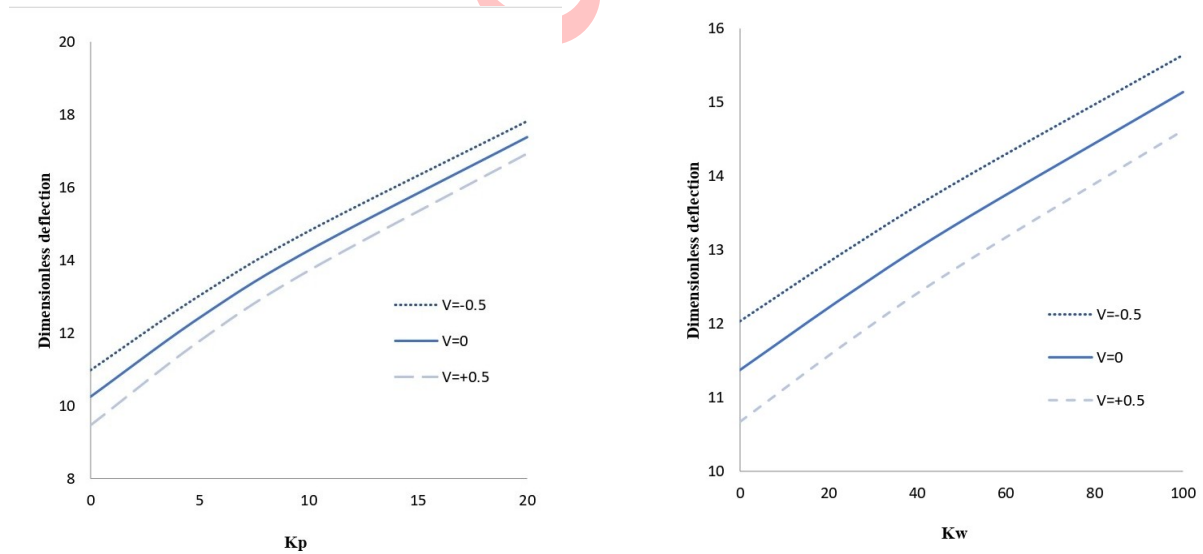


Figure 4: Effect of the Pasternak foundation on dimensionless deflection for a uniform load and various electric voltages ($L/h = 10, K_w = K_p = 20, \mu = 2, \Omega = 0, \Delta T = 20, \Delta H = 1$)

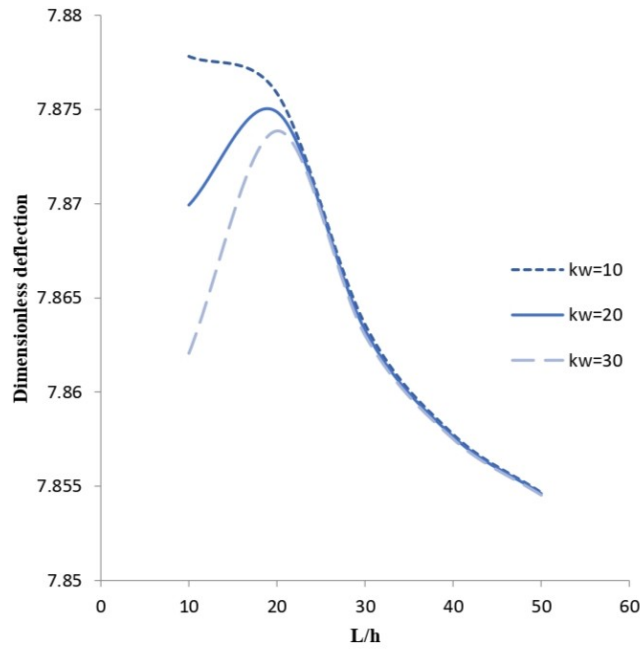


Figure 5: Effect of aspect ratio on dimensionless deflection for a uniform load and various Winkler foundation parameters ($L/h = 10, K_p = 20, V = 0, \Omega = 0, \Delta T = 20, \Delta H = 1$)

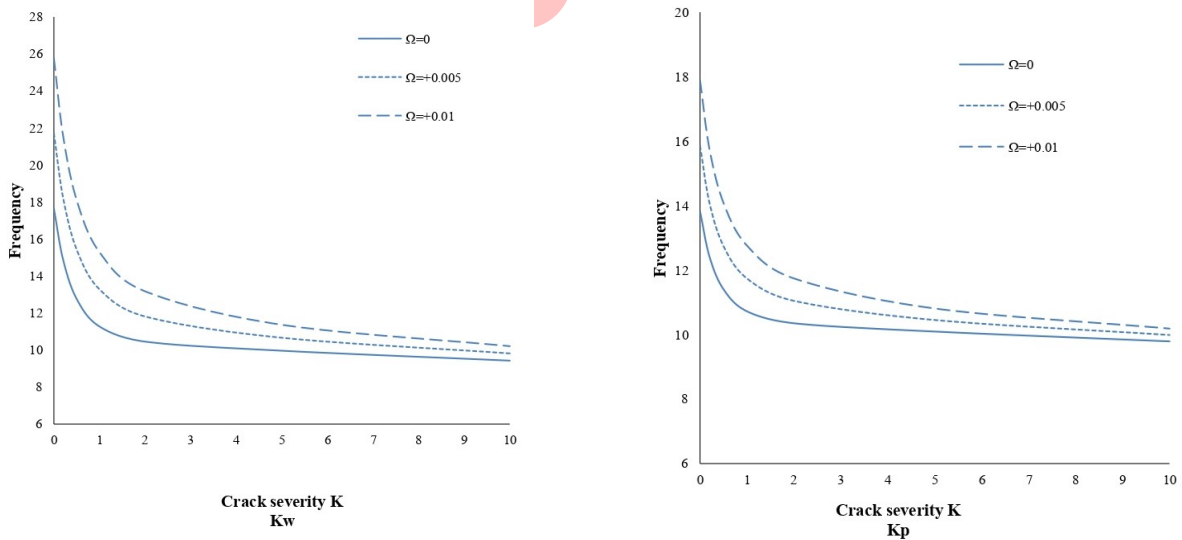


Figure 6: Effect of crack severity on frequency for various Winkler foundation parameters ($L/h = 10, K_p = K_w = 20, V = 0, \Delta T = 20, \Delta H = 1$)

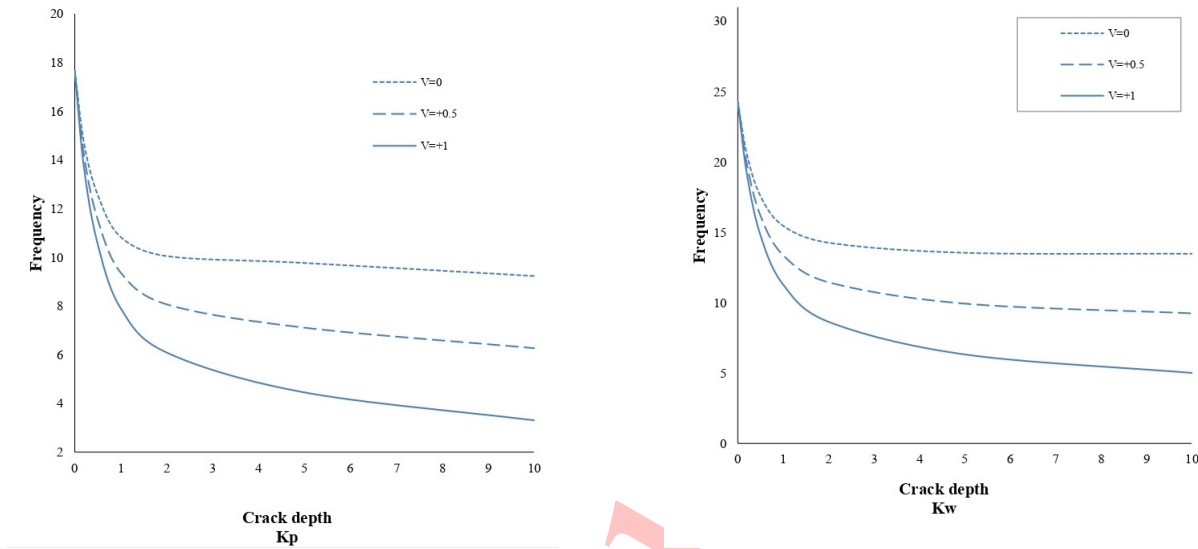


Figure 7: Effect of crack depth on frequency for various Winkler foundation parameters ($L/h = 10$, $K_p = K_w = 20$, $\Omega = 0$, $\Delta T = 20$, $\Delta H = 1$)

Fig. 3 presents the dimensionless deflection of the nanobeam as a function of slenderness ratio, considering a nonlocal scale parameter of $\mu = 2$. The bending of the nanobeam is observed to be amplified under the application of external electric voltage: specifically, negative voltages enhance deflection, while positive voltages reduce it. This indicates that positive and negative voltages induce axial tensile and compressive forces in the nanobeam, respectively. Additionally, it is observed that for zero electric voltage ($V = 0$), the dimensionless deflection remains nearly independent of the slenderness ratio.

Fig. 4 shows how the dimensionless deflection of nanobeams changes with Winkler and Pasternak foundation parameters under varying electric voltages and nonlocal parameters, for an aspect ratio of $L/h = 10$. Regardless of the polarity or level of applied voltage, an increase in dimensionless deflection is observed when larger Winkler and Pasternak parameters are used. The results also indicate that, under constant electric voltage, deflection is more sensitive to variations in the Pasternak parameter than in the Winkler parameter.

In Fig. 5, the influence of aspect ratio on the non-dimensional deflection of the nanobeam with varying Winkler foundation stiffness is illustrated. It is observed that as the aspect ratio (L/h) increases from 10 to 20, the dimensionless static deflection increases, but then decreases with further increase in aspect ratio. This behavior is attributed to the fact that increasing the Winkler foundation stiffness enhances the overall stiffness of the nanobeam, thereby reducing its deflection.

Fig. 6 shows the effect of crack severity on the natural frequency of the nanobeam for various magnetic potential and foundation stiffness values. The results indicate that an increase in magnetic potential leads to a reduction in frequency. Additionally, it is observed that the frequency decreases as crack severity increases. This trend can be attributed to the fact that higher Winkler foundation stiffness amplifies the influence of the crack more than Pasternak stiffness, thereby reducing the overall stiffness of the nanobeam and lowering its natural frequency.

Fig. 7 illustrates the effect of crack depth on the natural frequency of the nanobeam for different electric voltage and foundation stiffness values. The results show that increasing the applied electric

voltage leads to a decrease in frequency. It is observed that as the crack depth increases, the frequency initially rises and then gradually decreases. This behavior can be attributed to the fact that greater Winkler foundation stiffness amplifies the effect of crack depth, resulting in a reduction in the overall stiffness and dynamic response of the nanobeam.

7 Conclusion

The deflection characteristic of electro-magneto-elastic nanobeams under hygro-thermal conditions are analysed in the article. The governing equations are formulated through the application of Hamilton's principle, employing a higher-order refined beam model, and are solved analytically. A parametric investigation is conducted to assess the effects of the nonlocal parameter, thermal-moisture environment, coupled magneto-electro-mechanical loading, and aspect ratio on the deflection response. Significant influences are observed in terms of dimensionless deflection. Then both increasing aspect ratio and crack depth initially raise the nanobeam's natural frequency, followed by a decrease. This trend is influenced by Winkler foundation stiffness, which amplifies crack effects. As a result, overall beam stiffness and frequency are reduced.

8 Conflicts of interest

The authors declare that there are no conflicts of interest.

References

- [1] R.D. Adams, P. Pye, C.J. B.J. Stone, *A vibration technique for non-destructively assessing the integrity of structures*, J. Mech. Eng. Sci. **20** (1978) 93–100.
- [2] RA. Alghanmi, *Size-dependent static response of a functionally graded nanobeam attached to a piezoelectric fibre-reinforced composite actuator*, Sci. Rep. **15**(1) (2025) 28734.
- [3] M. Arefi, A.M. Zenkour, *A simplified shear and normal deformations nonlocal theory for bending of functionally graded piezomagnetic sandwich nanobeams in magneto-thermo-electric environment*, J. Sand. Struct & Mater. **18** (2016) 624–651.
- [4] M. Bastanfar, S.A.H. Hosseini, R. Sourki, F. Khosravi, *Flexoelectric and surface effects on a cracked piezoelectric nanobeam: Analytical resonant frequency response*, Arch. Mech. Eng. **66** (2019) 417–437.
- [5] O. Civalek, C. Demir, *Bending analysis of microtubules using nonlocal Euler–Bernoulli beam theory*, Appl. Math. Mod. **35** (2011) 2023–2067.
- [6] N. Challamel, C.M. Wang, *The small length scale effect for a non-local cantilever beam: a paradox solved*, Nanotechn. **99** (2008) 345703.
- [7] F. Ebrahimi, M.R. Barati, *Dynamic modeling of a thermo–piezo-electrically actuated nanosize beam subjected to a magnetic field*, Appl. Phy. **122** (2016) 451

- [8] F. Ebrahimi, M.R. Barati, *Dynamic modeling of a thermo-piezo-electrically actuated nanosize beam subjected to a magnetic field*, *Int. J. Smart & Nano Mater.* **7** (2016) 69–90.
- [9] F. Ebrahimi, S. Habibi, *Low-velocity impact response of laminated FG-CNT reinforced composite plates in thermal environment*, *Adv. Nano. Res.* **5** (2017) 69.
- [10] F. Ebrahimi, M.R. Barati, *Vibration analysis of smart piezoelectrically actuated nanobeams subjected to magneto-electrical field in thermal environment*, *J. Vib. Cont.* **24** (2018) 549–564.
- [11] A.C. Eringen, *Mechanics of Micromorphic Continua*, Springer-Verlag Berlin, Heidelberg. (1968) 18–35.
- [12] A.C. Eringen, *Nonlocal polar elastic continua*, *Int. J. Eng. Sci.* **10** (1972) 1–16.
- [13] A.C. Eringen, *Non-local polar field theory*, *Cont. Phy.* **4** (1976) 205–267.
- [14] A.C. Eringen, *Nonlocal Continuum Field Theories*, Springer, New York. (2002) 105.
- [15] A.C. Eringen, *Nonlocal continuum mechanics based on distributions*, *Int. J. Eng. Sci.* **44** (2006) 141–147.
- [16] J. Fernández-Sáez, R. Zaera, J.N. Reddy, *Bending of Euler–Bernoulli beams using Eringen’s integral formulation: A paradox resolved*, *Int. J. Eng. Sci.* **99** (2016) 107–116.
- [17] A. Ghorbanpour Arani, M.H. Zamani, *Investigation of electric field effect on size-dependent bending analysis of functionally graded porous shear and normal deformable sandwich nanoplate on silica Aerogel foundation*, *J. Sand. Struct. & Mater.* **21** (2019) 2700–2734.
- [18] N.A. Hussein, H.A. Rasul, S.S. Abdullah, *Free vibration analysis of multi-cracked nanobeam using nonlocal elasticity theory*, *Zanco. J. Pure Appl. Sci.* **32** (2020) 39–54.
- [19] L.L. Ke, Y.S. Wang, J. Yang, S. Kitipornchai, *Free vibration of size-dependent magneto-electro-elastic nanoplates based on the nonlocal theory*, *Acta. Mech. Sinica.* **30** (2014) 516–525.
- [20] P. Khodabakhshi, J.N. Reddy, *A unified integro-differential nonlocal model*, *Int. J. Eng. Sci.* **95** (2015) 60–75.
- [21] D.C.C. Lam, F. Yang, A.C.M. Chong, J. Wang, P. Tong, *Experiments and theory in strain gradient elasticity*, *J. Mech. Phys. Solids.* **51(8)** (2003) 1477–1508.
- [22] J. Loya, J. Lopez-Puente, J. Fernandez-Saez, *Free transverse vibrations of cracked nanobeams using a nonlocal elasticity model*, *J. Appl. Phys.* **105** (2009) 044309.
- [23] R.D. Mindlin, *Micro-structure in linear elasticity*, *Arch. Ration. Mech. Anal.* **16** (1964) 51–78.
- [24] A. Norouzzadeh, R. Ansari, *Finite element analysis of nano-scale Timoshenko beams using the integral model of nonlocal elasticity*, *Physica E* **88** (2017) 194–200.
- [25] A. Norouzzadeh, R. Ansari, H. Rouhi, *Pre-buckling responses of Timoshenko nanobeams based on the integral and differential models of nonlocal elasticity: an isogeometric approach*, *Appl. Phys. A* **5** (2017) 123–330.

- [26] A. Norouzzadeh, R. Ansari, H. Rouhi, *Nonlinear bending analysis of nanobeams based on the nonlocal strain gradient model using an isogeometric finite element approach*, Iran J. Sci. Technol. Trans. Civ. Eng. **43** (2019) 533–547.
- [27] A. Norouzzadeh, R. Ansari, H. Rouhi, *Nonlinear wave propagation analysis in Timoshenko nanobeams considering nonlocal and strain gradient effects*, Meccanica **53** (2018) 3415–3435.
- [28] K. Prashanthi, P.M. Sohrabi, T.S. Natarajan, T. Thundat, *Nanoscale magnetoelectric coupling in multiferroic BiFeO₃ nanowires*, Phys. Status Solid **6** (2012) 244–246.
- [29] J. Peddieson, G.R. Buchanan, R.P. McNitt, *Application of nonlocal continuum models to nanotechnology*, Int. J. Eng. Sci. **41** (2003) 305–312.
- [30] F. Pehlivan, I. Esen, K.G. Atkas, *Hermomechanical response of smart magneto-electro-elastic FGM nanosensor beams with intended porosity*, Arab. J. Sci. Eng. **50(4)** (2025) 2755–2777.
- [31] F. Ramirez, P.R. Heyliger, E. Pan, *Discrete layer solution to free vibrations of functionally graded magneto-electro-elastic plates*, Mech. Adv. Mater. Struct. **13** (2006) 249–266.
- [32] R. Selvamani, S. Mahesh, F. Ebrahimi, *Modified nonlocal couple stress problem of magneto thermoelasticity in a multilayered cylinder with Hall current, higher-order time derivatives and two-phase lags*, Acta Mech. **235** (2024) 4979–4992.
- [33] G.L. She, K.M. Yan, Y.L. Zhang, H.B. Liu, Y.R. Ren, *Wave propagation of functionally graded porous nanobeams based on non-local strain gradient theory*, Eur. Phys. J. Plus **133** (2018) 368.
- [34] M. Simsek, H.H. Yurtcu, *Analytical solutions for bending and buckling of functionally graded nanobeams based on the nonlocal Timoshenko beam theory*, Composit. Struct. **97** (2013) 378–386.
- [35] M. Sobhy, *Buckling and free vibration of exponentially graded sandwich plates resting on elastic foundations under various boundary conditions*, Composit. Struct. **99** (2013) 76–87.
- [36] J. Van den Boomgaard, D.R. Terrell, R.A.J. Born, H.F.J.I. Giller, *An in situ grown eutectic magnetoelectric composite material: Part I composition and unidirectional solidification*, J. Mater. Sci. **9** (1974) 1705–1709.
- [37] Y. Wang, J. Hu, Y. Lin, C.W.Nan, *Multiferroic magnetoelectric composite nanostructures*, NPG Asia Mater. **2** (2010) 61–68.
- [38] Y. Zhang, Y. Li, S. Li, *Free vibration of porous FG magneto-electro-elastic microbeams in the hygrothermal environment based on differential transformation method*, J. Intell. Mater. Syst. Struct. **35(3)** (2024) 253–269.
- [39] T. Zhao, L. Salamanca-Riba, H. Zheng, J. Wang, S.E. Lofland, Z. Ma, L. Mohaddes-Ardabili, S.R. Shinde, S.B. Ogale, F. Bai, D. Viehland, *Multiferroic BaTiO₃-CoFe₂O₄ nanostructure*, Science **303(5658)** (2004) 661–663.
- [40] Y.F. Zheng, Y. Zhou, F. Wang, C. Chen, *Nonlinear deformation analysis of magneto-electro-elastic nanobeams resting on elastic foundation by using nonlocal modified couple stress theory*, Eur. J. Mech. A/Solids **105158** (2024).